Microstructure, hardness homogeneity, and tensile properties of 1050 aluminum processed by constrained groove pressing

K. Hajizadeh[1] · S. Ejtemaei[2] · B. Eghbali[2]

Abstract 1050 commercial purity aluminum was subjected to severe plastic deformation through constrained groove pressing (CGP) at room temperature. Transmission electron microscope observations showed that after four CGP passes the majority of microstructure is composed of elongated grains/subgrains whose width/length average sizes are 506/1440 nm. This ultrafine-grained microstructure leads to a significant increase in yield strength of starting material from 93 to 182 MPa. At the same time, after four passes of CGP the material still displays a considerable ductility of 19%. Microhardness profiles reveal that average microhardness value in sample increases monotonically with increased straining during CGP. However, the degree of deformation homogeneity in samples remains almost unchanged at higher number passes. The latter was also confirmed by non-uniform distribution of imposed plastic strain in samples predicted by finite-element analysis.

✉ K. Hajizadeh
  kaveh.hajizadeh@uut.ac.ir

  S. Ejtemaei
  s.ejtemaei@gmail.com

  B. Eghbali
  eghbali@sut.ac.ir

[1] Faculty of Mining and Metallurgical Engineering, Urmia University of Technology, P.O. Box 57155-419, Urmia, Iran

[2] Faculty of Materials Engineering, Sahand University of Technology, P.O. Box 51335-1996, Tabriz, Iran

1 Introduction

During the past two decades, ultrafine-grained (UFG) materials have been the subject of huge interest due to their outstanding mechanical properties such as high strength, enhanced fatigue resistance and low-temperature superplasticity [1]. The most effective procedure for attaining ultrafine grains (less than 1 μm in diameter) in bulk materials is imposing intense plastic strain to them through methods known as severe plastic deformation (SPD) [1]. Until recently, numerous SPD techniques have been proposed but only few of them could be applied on sheet metals. These techniques include accumulative roll bonding (ARB) [2], asymmetric rolling (AR) [3], and constrained groove pressing (CGP) [4]. The bending of the rolled band and inhomogeneity of the strain distribution across the rolled bars thickness are two important issues limiting the application of asymmetric rolling [5]. On the other hand, ARB suffers from the bonding problems between two sheets which may degrade the mechanical properties of the processed materials [2]. By contrast, as an alternative method, constrained groove pressing proposed by Shin et al. [4] has a number of advantages. First, compared to asymmetric rolling CGP imposes more uniform shear deformation on the sheet metal [6]. Second, unlike the ARB process no bonding is necessary in this method. Third, it is a relatively inexpensive procedure so that it needs simple dies and it is easily performed on a wide range of metals using a hydraulic press that is readily available in most laboratories. A schematic presentation of the CGP process is shown in Fig. 1. A sheet sample of thickness t is located between a pair of asymmetric grooved dies (Fig. 1a) with groove angle of 45° and groove depth and width is same to sample thickness (t). Each pass of CGP includes four stages of pressing. As the dies press the
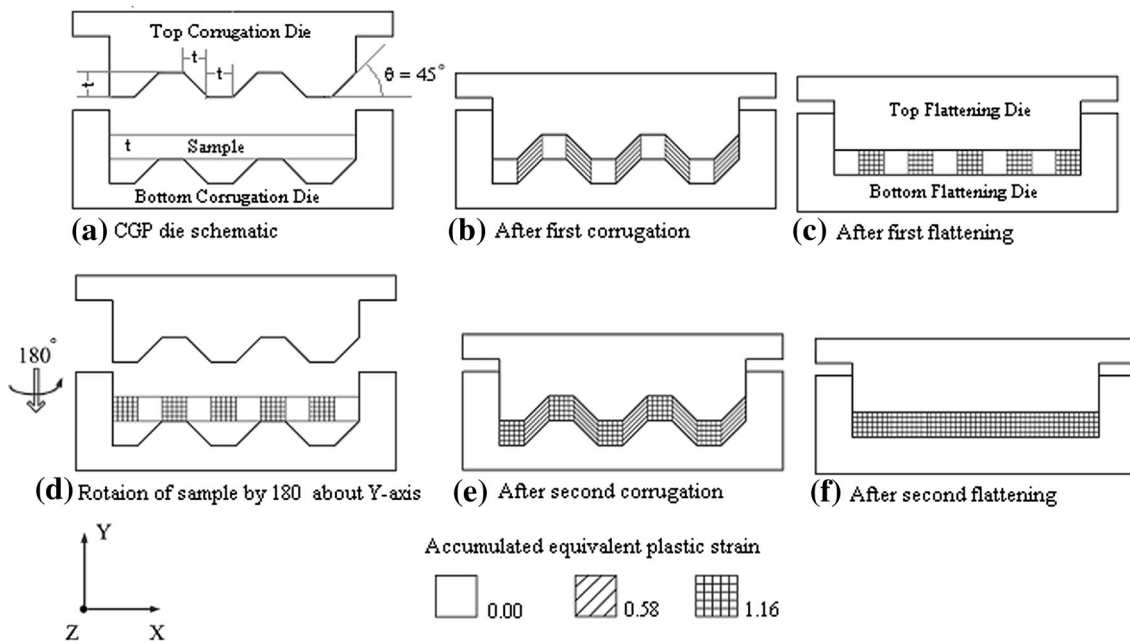
Fig. 1 Schematic illustration of the sequences of the CGP process

sample, the inclined regions of the sample (single-hatched regions in Fig. 1b) are subjected to shear deformation under the plane strain deformation condition and an equivalent plastic strain of 0.58 is imparted, whereas the flat regions (unhatched regions in Fig. 1b) remain unchanged. A pair of flat dies imposes a second pressing on the grooved sample (Fig. 1c) in which the deformed regions are subjected to the reverse shear deformation, leading to a total accumulated strain of 1.16, while the undeformed regions remain unchanged. By a 180 rotation of the sample (Fig. 1d) and successive pressing using a grooved and flat die (Fig. 1e), a homogeneous equivalent plastic strain of 1.16 is imposed throughout the sample after each pass (Fig. 1f). The repetition of the process is needed to obtain a large amount of imposed plastic strain and desired microstructural changes.

For Al sheets such CGP processing has been shown to produce a submicrometer order grain structure after total strain of 4.64 [4]. However, alloy chemistry plays a significant role in refinement of initial microstructure and obtaining a minimal grain size [1]. For example, the grain/subgrain size achieved in 99.99 wt% pure aluminum was reported to be 1 μm in [7] and 900 nm in [8] subjected, respectively, to four and five CGP passes. These values are quite large by comparison with 300 nm obtained in aluminum with purity of 99.64 wt% after four passes [9]. It has been proven that the mechanical properties of Al sheets could be considerably improved via CGP [4, 7–15]. However, depending on the impurity content of aluminum different trends have been observed in evolution of

hardness as well as tensile strength. In high-purity aluminum (99.9 wt%) the trend is such that the values of hardness, yield, and tensile strengths increase up to the second pass ($\varepsilon_{eff} = 2.32$) and reach to a maximum amount. Thereafter they show a slight decrease in subsequent passes [4, 7, 8]. When the purity of Al decreases, both the hardness and strength values after a rapid increase during initial passes either level off to a saturated value or increase continuously up to end of the process [9, 11].

Despite much activity in CGP processing of aluminum, only few researchers [4, 7–9, 12] investigated both the microstructure and mechanical properties of the processed material. Most of the earlier studies dealt merely with the deformation analysis using finite-element method (FEM) for establishing strain distribution characteristics [6, 16–18] or they focused on the evolution of mechanical properties [11, 14, 15]. Therefore, unlike ECAP, there are not enough evidences yet about the effect of impurity concentration on grain refinement and mechanical properties of pure aluminum.

This research is an attempt to study the microstructural features and mechanical properties of 1050 commercial purity aluminum after processing by CGP. Transmission electron microscopy (TEM) is used for microstructure observations. Hardness and tensile tests are utilized for evaluating the mechanical properties. Finite-element analysis is employed to attain plastic strain distribution and the obtained results are correlated with hardness of processed sample.

2 Experimental procedure

The material used in this study was 1050 commercial purity aluminum. The bulk chemical analysis of the as-received material is summarized in Table 1. Plates with dimensions of 40 mm × 50 mm × 5 mm were prepared from the as-received material. Prior to CGP, the plates were annealed at a temperature of 350 °C for 1 h to obtain a recrystallized structure. The initial average grain size was measured to be about 80 μm.

CGP was conducted up to four passes, corresponding to an equivalent strain of 4.64, on a 150 ton hydraulic press at room temperature. The plates were coated with a graphite base lubricant before pressing to reduce the frictional effects and the pressing was carried out at a constant press speed of 2 mm s^{-1}.

The microstructure of deformed samples was examined by transmission electron microscopy (TEM) using a JEOL JEM 1200EX electron microscope operated at 120 kV. Thin foils for TEM were first mechanically polished and finally electropolished in a Tenupol 5 double-jet polishing unit using a mixture of 25% nitric acid and 75% methanol at an applied potential of 25 V and at −30 °C. TEM observations were made on transverse cross section (the section which is perpendicular to the grooves of CGP-ed samples).

Microhardness and tensile tests were carried out to evaluate the strength and ductility of the processed material. Vickers microhardness (Hv) was carried out using a microhardness tester Future-Tech FM-700 along the central line of the transverse cross section by imposing a load of 300 g for 10 s. The first point for microhardness test was 2.5 mm far from the edge of specimen and other points were located 3 mm far from each other. Room temperature tensile tests were conducted on the CGP-ed plates using a Zwick/Roell Z010 testing machine at an initial strain rate of 2.7×10^{-4} s^{-1}. Tensile test specimens were cut such that their gage length aligned parallel to the grooves. Experiments were repeated on two to three companion specimens to check repeatability.

Table 1 Chemical composition of 1050 Al utilized in the present study

Element	Mass percentage (wt%)
Al	99.5
Si	0.1
Fe	0.22
Mn	0.03
Cu	0.002
Mg	0.006

To explain the microhardness profiles measured from the transverse section finite-element analysis was carried to predict the plastic strain distributions in samples. For this purpose, commercial software ABAQUS/CAE 6.9-1 was used. In simulations, dies were assumed to be discrete rigid meaning there is no deformation. The pressing speed and coefficient of friction between the die and specimen were taken to be 2 mm s^{-1} and 0.1, respectively. The aluminum specimens fit to the category of elasto-plastic material with isotropic hardening. Tensile tests were used to define the plastic behavior of the material during finite-element simulations. To cover the large amounts of equivalent plastic strain imposed to the material in CGP process, not only the stress–strain curve of undeformed material but also those of CGP processed samples were determined and used. Figure 2 presents the reference true stress versus true plastic strain curve that is introduced to Abaqus as a classical metal plasticity model. The specimens were meshed by total number of 1000 two-dimensional plane strain (CPE4) elements.

3 Results

3.1 Microstructure observations

Figure 3 shows typical TEM microstructures of aluminum after four passes of CGP taken from the transverse section of a processed plate. As expected, during straining to a level of 4.46 the initial coarse-grained structure underwent a significant refinement from tens of microns down to submicrometer range. Most of the grains showed a short, elongated morphology and their average aspect ratio was
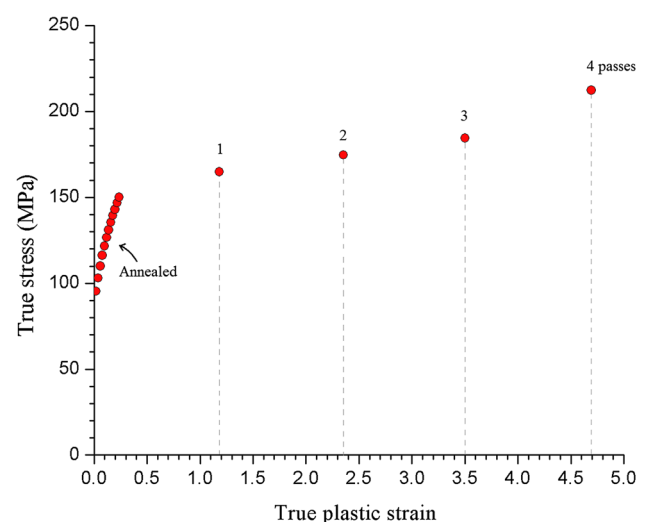
Fig. 2 Hardening curve of 1050 Al obtained by tensile tests on the annealed material as well as on the samples processed by CGP for different number of passes
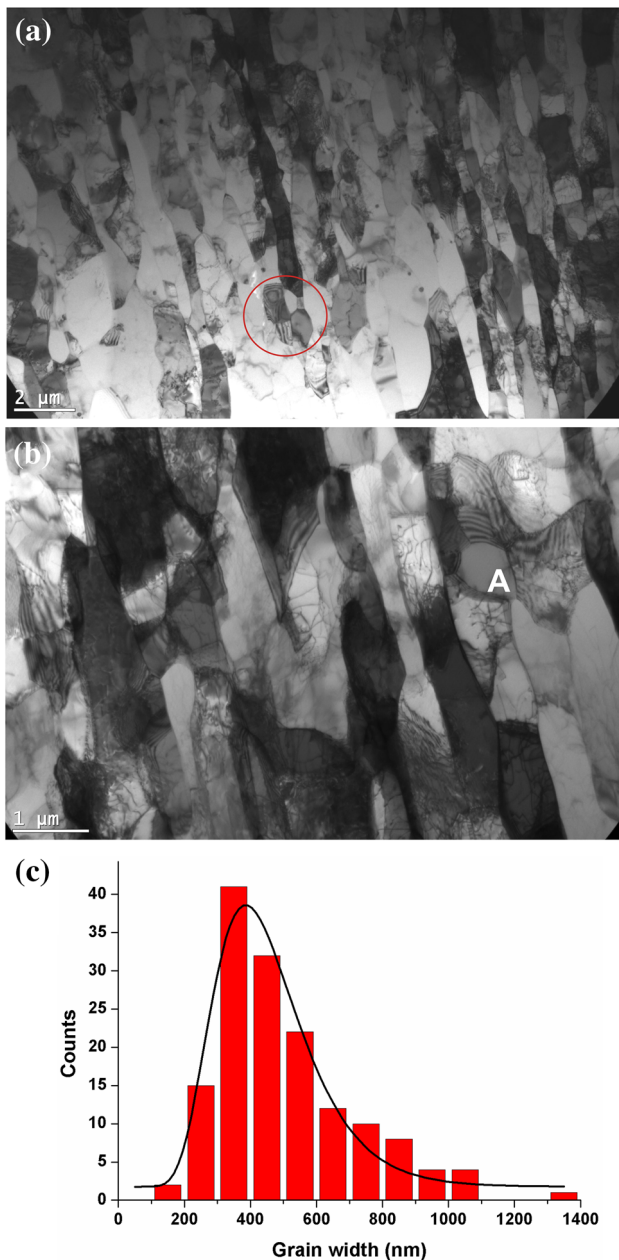
Fig. 3 Bright-field TEM micrographs and grain size distribution of 1050 Al after processing by four passes of CGP. **a** Low and **b** high magnifications, **c** grain size distribution histogram

measured to be 3.1. Some well-developed equiaxed grains, e.g., ones encircled on Fig. 3a can be also detected which were probably formed by the fragmentation of elongated grains. The high-magnification image (Fig. 3b) shows that dislocation density is relatively high. But distribution of dislocations is non-uniform. While some grains are nearly free of lattice dislocations, e.g., the grain marked as A, some others do have dislocation tangles and cell structures in the grain interior. Such inhomogeneous structures are typical of SPD-processed materials, as discussed in Ref.

[19]. As shown in Fig. 3b, most of the grain boundaries are sharp and clear and the difference in contrast between neighboring grains is large, thereby suggesting that the misorientation angles between adjacent grains are relatively high. The width of elongated grain/subgrains (Fig. 3c) varies dramatically from 96 to 1361 nm and the width/length average sizes were measured to be 506 and 1440 nm, respectively. The solid line of log-normal distribution in Fig. 3c can be used to conclude that the experimental grain/subgrains width distribution is close to log-normal.
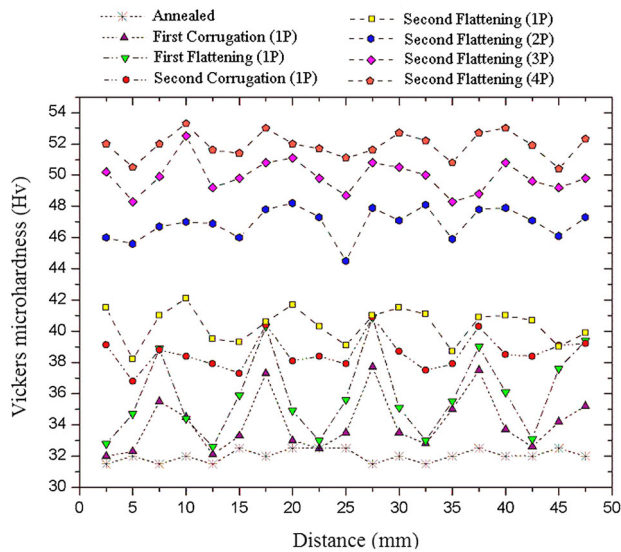
3.2 Hardness

The average values of the Vickers microhardness are shown in Fig. 4 for the annealed sample and after processing by CGP for up to four passes. It is apparent that the average microhardness increases from Hv = 32 for the as-annealed condition to Hv = 40 after a single pass of CGP and enhances to Hv = 47 in the second pass. Thereafter, it increases slightly to a maximum value of Hv = 52 after a total of four passes.

To examine the deformation homogeneity obtained during CGP, the microhardness measurements recorded along the central line on transverse cross section are plotted against the distance in Fig. 5. It is apparent that the annealed Al sample exhibits a relatively uniform hardness distribution. After the first corrugation, periodic fluctuations are appeared and become even more severe during the flattening stage. By contrast, second corrugation and flattening improves the deformation homogeneity. This is
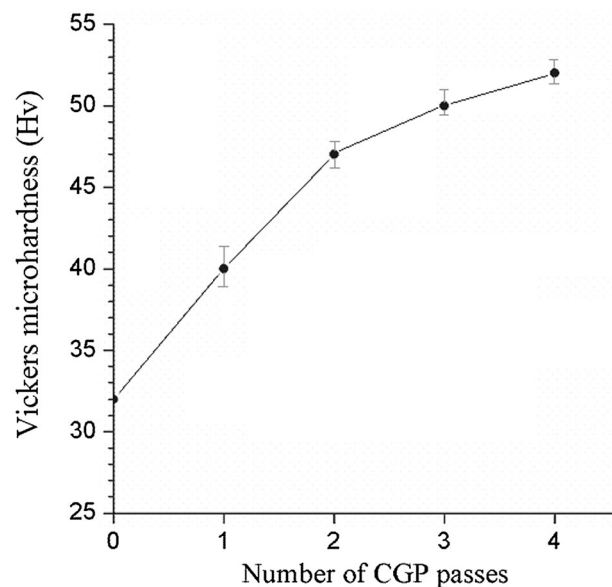
Fig. 4 Vickers microhardness variation in 1050 Al with respect to number of CGP passes

Fig. 5 Vickers microhardness profile recorded along the transverse cross section of the samples

Fig. 6 Equivalent plastic strain contours in samples after different stages of CGP predicted from FEM
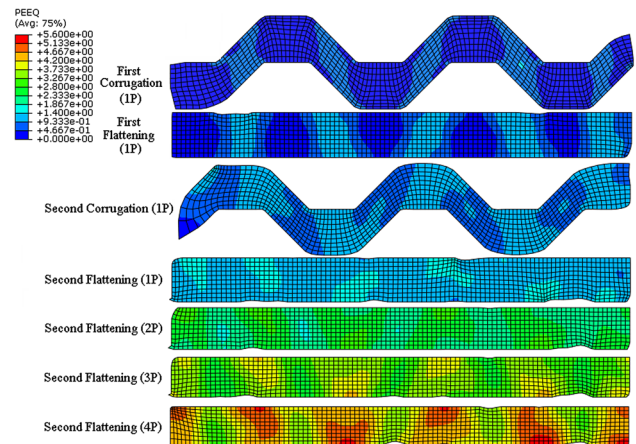
suggested by a more uniform hardness distribution along the sample length.

Although the average Hv values are increased with the increasing number of passes, it is seen in Fig. 5 that the microhardness distribution followed almost the same trend observed after the first pass and, therefore, deformation homogeneity does not improve remarkably even after higher number of CGP passes. This behavior may be explained by having knowledge of strain distribution in sample which can be attained by finite-element analysis. That is why, finite-element simulations were carried out in this study.
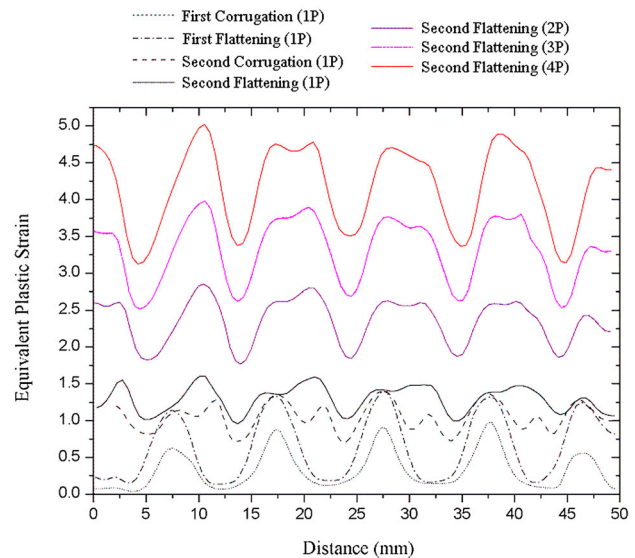
3.3 Finite-element analysis

As mentioned previously a single pass of CGP comprises four alternating corrugation and flattening stages. In this regard, Fig. 6 illustrates the simulated distribution of equivalent plastic strain in sample after these stages during the first pass as well as after completion of subsequent passes.

In Fig. 6 it is obviously seen that during each CGP stage, the plastic strain is not distributed uniformly throughout the sample. To examine the strain distribution more closely, equivalent plastic strain along the central line of transverse cross section has been plotted against the distance in Fig. 7. Inspection of this figure reveals that after the first corrugation, regular periodic fluctuations have appeared and their amplitude increases during the flattening stage. After the second corrugation, minor peaks appear in the shearing regions (which were previously undeformed flat regions) and these peaks intensify during the second flattening stage.


Fig. 7 The distribution of equivalent plastic strain along the central line of transverse cross section of samples after different stages of CGP predicted from FEM

3.4 Tensile properties

Figure 8 shows the room temperature engineering stress–strain curves obtained by tensile tests for the starting material and CGP processed samples after different number of passes. The tensile properties determined from the stress–strain curves are summarized in Table 2. It is seen that the yield (σ_y) and ultimate tensile strength (σ_{UTS}) of 1050 aluminum rapidly increase after the first pass and reach as high as 147 and 160 MPa, respectively. These are significantly higher than the values obtained in the initially annealed material ($\sigma_y = 93$ and $\sigma_{UTS} = 118$ MPa). In subsequent passes, the strength improves gradually and its increment is comparatively low. The same trend was also
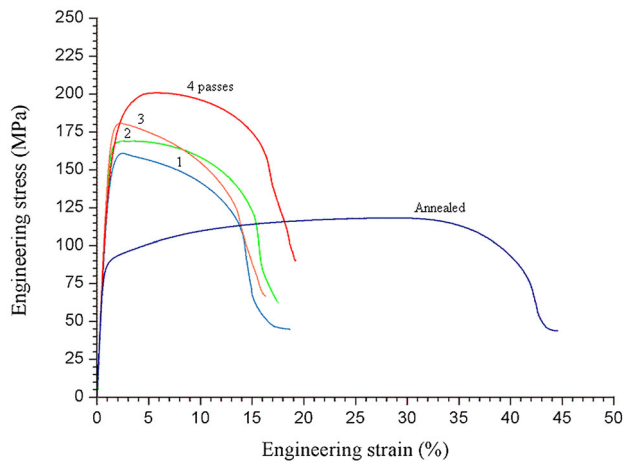
Fig. 8 Tensile engineering stress–strain curves of 1050 Al processed by CGP for different number of passes

observed previously in evolution of microhardness after different number of CGP passes as shown in Fig. 4.

In terms of ductility, one pass CGP-ed sample shows a total elongation of 19% which is remarkably lower than the value related to the starting material (about 45%). The additional deformation up to three passes leads to a gradual decrease in ductility to about 16.5%. However, after four passes the ductility tends to improve and reaches 19%. In general, processing four passes by CGP resulted in a significant increase in the values of yield strength by 95% from 93 to 182 MPa and ultimate tensile strength by 70% from 118 to 200 MPa. These improvements in strength values are accompanied with decrease in ductility wherein elongation to failure decreases from 45% in the annealed condition to 19% after four passes of CGP.

4 Discussion

4.1 Microstructure refinement

The grain subdivision which takes places during plastic deformation of metals with high stacking fault energy like aluminum is performed by dislocation activities. Gliding, accumulation, interaction, tangling, rearrangement, and annihilation of dislocations form dislocation cells (DCs) inside initial coarse grains [20]. Transformation of DC

walls into sub-boundaries with small misorientation angles and evolution of sub-boundaries into high-angle boundaries occur following straining [20]. Although with increasing strain the microscopic subdivision occurs on a finer and finer scale, i.e., new and finer DCs are continuously formed and evolve to subgrain/grain structure, with the increment of deformation strain, grain subdivision does not continue indefinitely. Many researchers have confirmed that grain size refinement during SPD eventually saturates after a given amount of imposed strain [1, 21, 22]. Deformation temperature, alloy chemistry, strain path, and strain rate are the dominant factors controlling the obtained saturation grain size in single-phase materials [22].

As seen in sections of 3.2 and 3.4 no tendency to saturate in mechanical properties was observed in studied material even after four passes. This indicates that the grain size refinement still continues. In practice, however, deformation of Al by CGP to very high strains wherein more refinement can be obtained leads to failing of samples. For this reason, similar to the most of earlier works, in this study samples could be successfully pressed just up to four passes (ε_{eff} = 4.64).

The average grain/subgrain size obtained in this study is almost half of those already reported for 99.9 wt% purity Al (1 µm [7] and 900 nm [8]), demonstrating the effectiveness of impurity content on degree of grain refinement. As mentioned previously the aluminum used in this study was a commercial purity grade with purity level of 99.5 wt%. Impurities may exist in the form of solute atoms or precipitates either inside grains or at the grain boundaries. During deformation, those existing inside grains can restrict dislocation motion and hence retard dislocation annihilation. As a result, dislocation density increases in grain interior and hence they are positioned closer together. Under these conditions, it is reasonable to consider that the tangling of dislocations to take place in closer distances and eventually lead to formation of a finer grain structure with increasing strain. At the same time, the segregation of impurities to the freshly formed grain/subgrain boundaries can impede the migration of these boundaries and thereby inhibit the grain growth [23]. It is noted that the grain growth is commonly observed during SPD of high-purity aluminum when the deformation is continued to impose very large strains [24].

Table 2 Mechanical properties of 1050 Al after processing by CGP

Processing conditions	σ_y (MPa)	σ_{UTS} (MPa)	ε_f (%)	ε_u (%)	Vickers microhardness (Hv)
As-annealed	93	118	45	31	32
CGP-1 pass	147	160	19	2.5	40
CGP-2 passes	152	168	17.7	3.4	47
CGP-3 passes	167	180	16.5	2.3	50
CGP-4 passes	182	200	19	5.8	52

On the other hand, when compared with other SPD methods, the average grain/subgrain size of 506 nm obtained in this study is still significantly larger than $d = 350$ nm attained in 1050 aluminum processed by ECAP for a total of eight passes using route B_C [25]. This discrepancy shall be attributed first to the higher amount of plastic strain (~ 8) which was imparted to the material during ECAP. In addition, it is noted that the strain pass experienced by sample in CGP differs from that of ECAP. The inherent nature of CGP process which involves reversal of loading direction after each stage of pressing leads to relatively lower grain refinement when compared to other SPD methods such as ECAP and ARB [26]. This is because dislocations formed in previous pressing stage (corrugation) have high chance to meet dislocations with opposite signs or with opposite twisting directions in the same shear plane during next pressing stage (flattening), leading to their annihilation [8]. This results in less accumulation of dislocations inside grains and causes the delay of grain subdivision and UFG formation.

4.2 Hardness evolution and its correlation with results of FEM analysis

The data presented in Fig. 4 demonstrate that the hardness of deformed samples increases monotonically with the number of CGP passes. Although the rate of the increment is reduced, no saturation was attained in CGP at least up to four passes. The same trend has been also reported by some other researchers where the purity level of studied Al was relatively lower, about 99.2 wt% [10, 11]. However, with increasing purity, hardness tends to saturate, as it was found for 99.64 wt% Al in [9], or reaches to a maximum followed by a slight drop in subsequent passes, similar to that observed in high-purity 99.99 wt% Al in [4] and [8]. As seen, the evolution of hardness with imposed strain during CGP is strongly associated with the impurity level of aluminum. It should be emphasized that a larger amount of impurities and solute atoms in Al reduces the mobility of dislocations and has a negative effect on the progress of dynamic recovery. As a result, they delayed the occurrence of saturation state. On the other hand, the failing of samples which often takes place in higher number of passes does not allow imposing very large strains. Thus, the saturation has a little chance to be observed in lower purity grades of Al during CGP.

The high rate of increase in hardness at the initial passes can be associated with the strain hardening effect as a result of increased dislocation density and subgrain boundaries formation. During the further CGP passes, misorientation angles associated with sub-boundaries are gradually enlarged due to absorption of more lattice dislocations [1]. This phenomenon in turn decreases the rate of dislocation density increasing with strain because the grain boundary area acts as a dislocation sink and consumes dislocations. As a consequence, the role of strain hardening mechanism would be gradually weakened. Instead, grain boundary hardening–strengthening would begin to dominate. This causes that the hardness continues to increase but at a slower rate than initial passes.

The observed fluctuations in strain distribution in Fig. 7 are due to the fact that during every deformation stage the central points of the shear regions receive maximum shear deformation but the central points of flat regions still remain undeformed. Regions between these two points are subjected to shear deformation between zero and the maximum values and with moving from center of shear region towards flat region the imposed strain decreases. This leads to formation of peaks and valleys in the strain distribution curve. Since during the second corrugation and flattening stages the former flat regions become new shear regions and undergo shear deformation, the interface region between the shear and flat regions will receive minimum deformation during each pass of CGP. As a result, one can say that the valleys observed in the strain distribution curves correspond to the strain values of interface regions, whereas the peaks correspond to the shear/flat regions.

As can be seen in Fig. 7, the strain distribution in sample has followed the same trend in next CGP passes, i.e., a relatively regular periodic curve like the one that appeared after completion of the first pass is observed after second corrugation stage in all the following passes. In addition, as expected the strain level imposed on the sample increases gradually with increasing CGP pass number. By comparing Figs. 5 and 7 and considering the fact that higher hardness is expected at regions where higher strain is accumulated, the non-uniform distribution of hardness along the sample length is in good agreement with the strain distribution predicted by finite-element analysis (Fig. 7).

4.3 Evolution of strength and ductility

Similar to microhardness, increase in tensile strength during CGP could be ascribed to increment in dislocation density and its relevant work hardening as well as to the grain refinement. Both of these factors necessitate higher applied stress for dislocation motion by slip [27]. It is apparent from Fig. 8 that the stress–strain curves of 1050 Al after CGP show peak stress at early stages of the tensile test, resulting in smaller values of uniform plastic strain (below 6%) compared to that of annealed material ($\sim 31\%$). Despite this limitation, which arises from their low strain hardening capacity [28, 29], CGP-ed samples exhibited relatively high magnitudes of total strain (16.5–19%). This behavior may be explained on the base of

elevated strain rate sensitivity (m in Holloman's relation [27]) of processed material [21, 30–32]. As seen in Fig. 8, the post-uniform elongation has a major contribution in ductility of CGP-ed samples. It is noted that in tensile tests, after the maximum load, the non-uniform plasticity depends on the strain rate sensitivity [29]. The onset of necking leads to locally high strain rates and, for a high value of m, results in a sharp increase in the yield stress inside the necked region. This delays the neck development, allowing additional deformation outside the neck and results in a large non-uniform elongation.

The data presented in Table 2 demonstrate that increasing CGP passes up to three leads to an increase in the yield and tensile strengths but decreases the ductility. Nevertheless, when pressing is continued to a total of four passes, it is interesting to note that not only strength but also ductility increases. This is an unexpected matter. However, it seems that it is associated with an increase in strain hardening capability of processed sample which delayed the onset of necking and thereby made a contribution to the total elongation. It is seen in Table 2 that while the magnitude of uniform elongation is equal to 2.3 for three-pass-processed sample, it markedly increased after four passes and reached 5.8. Similar trend has been already reported for copper where a simultaneous enhancement in strength and ductility was observed with increase in number of ECAP passes [33]. This behavior has been explained on the base of increase in the fraction of high-angle grain boundaries with increasing imposed strain and consequently with an increasing role of grain boundary sliding and grain rotations as mechanisms accommodating plastic deformation [21, 33].

5 Conclusion

Constrained groove pressing (CGP) was conducted on 1050 commercial purity aluminum up to four passes ($\varepsilon_{eff} = 4.64$) and the following results are obtained:

1. An ultrafine-grained microstructure consisting of mainly elongated grains/subgrains whose width/length average sizes are 506 and 1440 nm, respectively, is achieved in aluminum after four CGP passes. The average grain/subgrain size obtained in this study is almost half of those already reported for 99.9 wt% purity Al, demonstrating the effectiveness of impurity content on degree of grain refinement.

2. Formation of the UFG structure in aluminum results in a significant improvement in:

   (a) microhardness by about 62% from 32 to 52 Hv,
   (b) yield strength by 95% from 93 to 182 MPa, and
   (c) ultimate tensile strength by 70% from 118 to 200 MPa.

3. The microhardness and strength increase continually with increasing number of CGP passes and no saturation is observed.

4. Ductility decreases until pass three as the number of passes increases. After that it interestingly increases to 19%. This increase is accompanied by a considerable restoration of work hardening ability of processed sample.

5. The Vickers microhardness exhibits a relatively inhomogeneous distribution along the transverse cross section of sample after a single pass. The degree of hardness homogeneity does not improve remarkably with more straining during next passes. This is consistent with simulated non-uniform strain distribution in sample obtained by FEM.

References

1. R.Z. Valiev, R.K. Islamgaliev, I.V. Alexandrov, Prog. Mater Sci. **45**, 103 (2000)
2. Y. Saito, H. Utsunomiya, N. Tsuji, T. Sakai, Acta Mater. **47**, 579 (1999)
3. Y.H. Ji, J.J. Park, Mater. Sci. Eng. A **499**, 14 (2009)
4. D.H. Shin, J.J. Park, Y.S. Kim, K.T. Park, Mater. Sci. Eng. A **328**, 98 (2002)
5. S.A.A. Akbari Mousavi, S.M. Ebrahimi, R. Madoliat, J. Mater. Process. Technol. **187–188**, 725 (2007)
6. M.S. Ghazani, A. Vajd, Model. Simul. Mater. Sci. Eng. **4**, 32 (2014)
7. J. Zrnik, T. Kovarik, Z. Novy, M. Cieslar, Mater. Sci. Eng. A **503**, 126 (2009)
8. S.S. Satheesh Kumar, T. Raghu, Mater. Des. **57**, 114 (2014)
9. S. Morattab, K. Ranjbar, M. Reihanian, Mater. Sci. Eng. A **528**, 6912 (2011)
10. A. Krishnaiah, U. Chakkingal, P. Venugopal, Scr. Mater. **52**, 1229 (2005)
11. A. Shirdel, A. Khajeh, M.M. Moshksar, Mater. Des. **31**, 946 (2010)
12. E. Hosseini, M. Kazeminezhad, Mater. Sci. Eng. A **526**, 219 (2009)
13. M. Borhani, F. Djavanroodi, Mater. Sci. Eng. A **546**, 1 (2012)
14. A. Sajadi, M. Ebrahimi, F. Djavanroodi, Mater. Sci. Eng. A **552**, 97 (2012)
15. J.W. Lee, J.J. Park, J. Mater. Process. Technol. **130–131**, 208 (2002)
16. S.C. Yoon, A. Krishnaiah, U. Chakkingal, H.S. Kim, Comput. Mater. Sci. **43**, 641 (2008)
17. S.S. Satheesh Kumar, I. Balasundar, T. Raghu, Int. J. Comput. Mater. Sci. Eng. **2**, 1 (2013)
18. Y.T. Zhu, J.Y. Huang, J. Gubicza, T. Ungar, Y.M. Wang, E. Ma, R.Z. Valiev, J. Mater. Res. **18**, 1908 (2003)

19. B. Bay, N. Hansen, D.A. Hughes, D. Kuhlmann-Wilsdorf, Acta Metall. Mater. **40**, 205 (1992)
20. R.Z. Valiev, T.G. Langdon, Prog. Mater Sci. **51**, 881 (2006)
21. R. Pippan, S. Scheriau, A. Taylor, M. Hafok, A. Hohenwarter, A. Bachmaier, Annu. Rev. Mater. Res. **40**, 319 (2010)
22. X. Sauvage, G. Wilde, S.V. Divinski, Z. Horita, R.Z. Valiev, Mater. Sci. Eng. A **540**, 1 (2012)
23. M. Kawasaki, Z. Horita, T.G. Langdon, Mater. Sci. Eng. A **524**, 143 (2009)
24. P.L. Sun, P.W. Kao, C.P. Chang, Metall. Mater. Trans. A **35A**, 1359 (2004)
25. K. Peng, Y. Zhang, L.L. Shaw, K.W. Qian, Acta Mater. **57**, 5543 (2009)
26. G.E. Dieter, *Mechanical Metallurgy* (McGraw Hill, Singapore, 1998)
27. D. Jia, Y.M. Wang, T. Ramesh, E. Ma, Y.T. Zhu, R.Z. Valiev, Appl. Phys. Lett. **79**, 611 (2001)
28. Y.M. Wang, E. Ma, Acta Mater. **52**, 1699 (2004)
29. R.Z. Valiev, J. Mater. Sci. **42**, 1483 (2007)
30. J. May, H.W. Hoppel, M. Goken, Scr. Mater. **53**, 189 (2005)
31. K. Hajizadeh, B. Eghbali, K. Topolski, K.J. Kurzydlowski, Mater. Chem. Phys. **143**, 1032 (2014)
32. R.Z. Valiev, I.V. Alexandrov, T.C. Lowe, Y.T. Zhu, J. Mater. Res. **17**, 5 (2002)
33. X.Z. Liao, Y.H. Zhao, Y.T. Zhu, R.Z. Valiev, D.V. Gunderov, J. Appl. Phys. **96**, 636 (2004)